Electronic supplementary information (ESI)

Structural and magnetic properties of lanthanide - tetraphenol complexes based cyclen: slow magnetic relaxation of the Nd^{III} compound

Salah S. Massoud [a,b*], Febee R. Louka [a], Thierry Guizouarn [c], Roland C. Fischer [d*], Ana Torvisco [d], Franz A. Mautner [e], Asia M. Smith [a], Nahed M. H. Salem,[b] Gunasekaran Velmurugan [f], Peter Comba [f*] and Fabrice Pointillart [c*]

[a] Department of Chemistry, University of Louisiana at Lafayette, P.O. Box 43700, Lafayette, LA 70504, U.S.A.

[b] Department of Chemistry, Faculty of Sciences, Alexandria University, Moharam Bey 21511, Alexandria, Egypt.

[c] Univ Rennes, CNRS, ISCR (Institut des Sciences Chimiques de Rennes) – UMR 6226, 35000 Rennes, France; fabrice.pointillart@univ-rennes.fr

[d] Institute of Inorganic Chemistry, Graz University of Technology, Stremayrgasse 9, A-8010 Graz, Austria; roland.fischer@tugraz.at

[e] Institute of Physical and Theoretical Chemistry, Graz University of Technology, Stremayrgasse 9, A8010 Graz, Austria.

[f] Anorganisch-Chemisches Institut, and Interdisziplinäres Zentrum für Wissenschaftliches Rechnen (IWR), Universität Heidelberg, Im Neuenheimer Feld 270,69120 Heidelberg, Germany.

Content **page #**

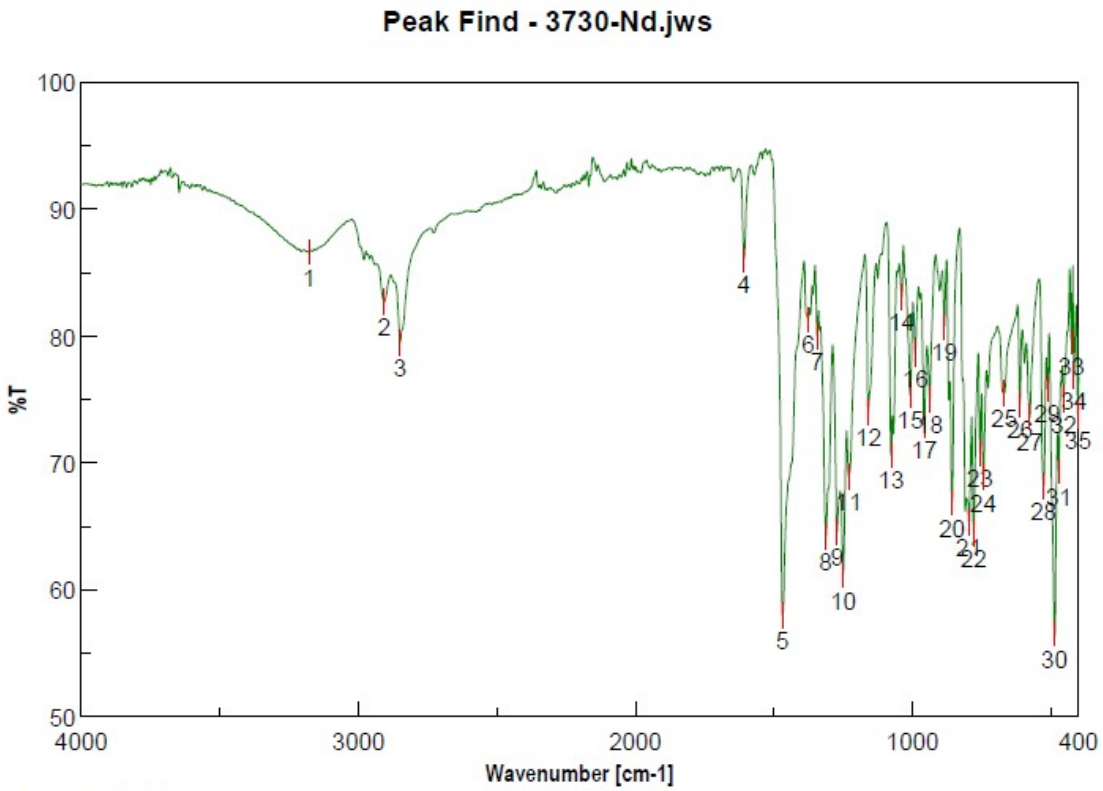

[Result of Peak Picking]

No.	Position	Intensity	No.	Position	Intensity
1	3179.08	87	2	2907.16	83
3	2849.31	80	4	1607.38	86
5	1469.49	58	6	1376.93	81
7	1344.14	80	8	1312.32	64
9	1271.82	65	10	1249.65	61
11	1230.36	69	12	1159.01	74
13	1077.05	71	14	1039.44	83
15	1007.62	75	16	990.268	79
17	957.484	73	18	937.235	75
19	885.166	81	20	857.204	67
21	795.493	65	22	779.101	64
23	755.959	71	24	743.424	69
25	669.178	75	26	612.288	75
27	576.612	74	28	526.471	68
29	512.972	76	30	487.902	57
31	471.51	69	32	454.154	75
33	426.191	80	34	416.549	77
35	402.085	74			

Fig. S1. IR spectrum of complex **1**

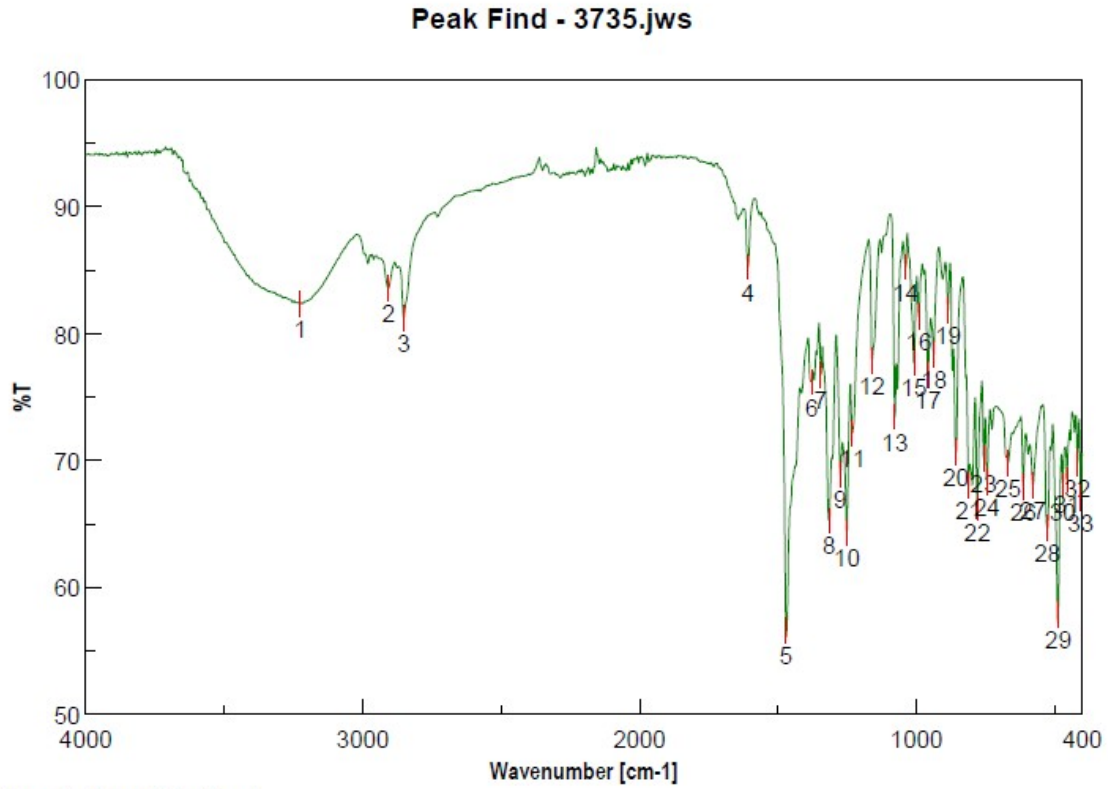

[Result of Peak Picking]

No.	Position	Intensity	No.	Position	Intensity
1	3226.33	82	2	2907.16	84
3	2852.2	81	4	1608.34	85
5	1471.42	57	6	1378.85	76
7	1345.11	77	8	1316.18	65
9	1274.72	69	10	1251.58	64
11	1231.33	72	12	1159.97	78
13	1078.01	73	14	1039.44	85
15	1008.59	78	16	991.232	81
17	958.448	77	18	937.235	78
19	886.131	82	20	856.239	71
21	811.885	68	22	780.065	66
23	756.923	70	24	744.388	68
25	668.214	70	26	614.217	68
27	578.54	68	28	526.471	65
29	487.902	58	30	470.546	68
31	456.082	68	32	417.513	70
33	405.942	67			

Fig. S2. IR spectrum of complex **2**

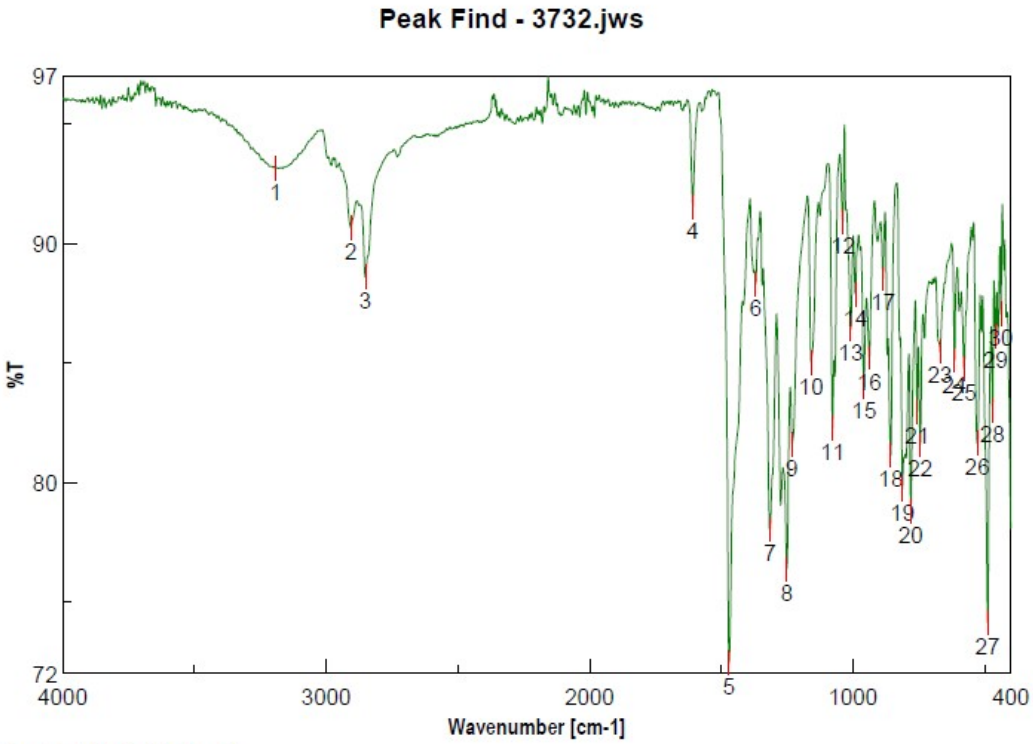

[Result of Peak Picking]

No.	Position	Intensity	No.	Position	Intensity
1	3191.61	93	2	2907.16	91
3	2851.24	89	4	1608.34	92
5	1470.46	72	6	1369.21	88
7	1315.21	78	8	1251.58	76
9	1231.33	82	10	1159.01	85
11	1078.01	82	12	1038.48	91
13	1008.59	86	14	991.232	88
15	958.448	84	16	938.199	85
17	886.131	89	18	856.239	81
19	811.885	80	20	780.065	79
21	756.923	83	22	745.352	82
23	669.178	85	24	615.181	85
25	578.54	85	26	528.4	82
27	488.866	74	28	470.546	83
29	458.975	86	30	438.726	87

Fig. S3. IR spectrum of complex **3**

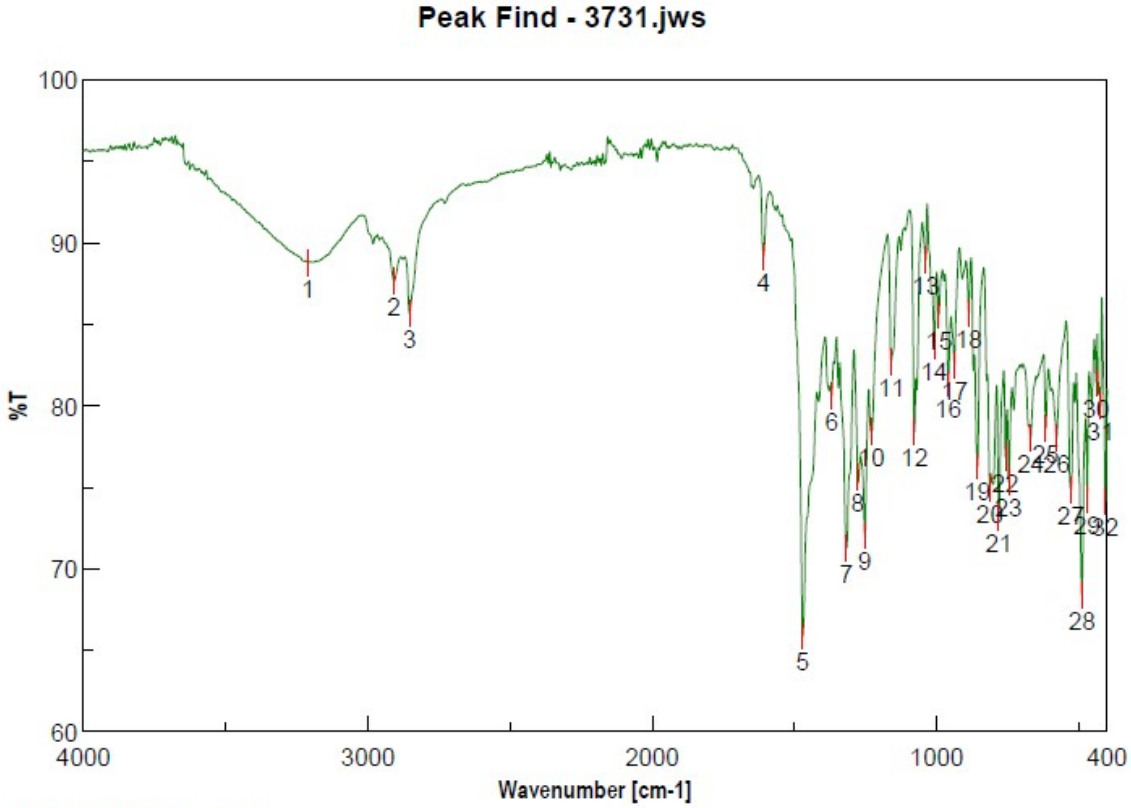

[Result of Peak Picking]

No.	Position	Intensity	No.	Position	Intensity
1	3210.9	89	2	2908.13	88
3	2853.17	86	4	1608.34	89
5	1470.46	66	6	1369.21	81
7	1317.14	71	8	1277.61	76
9	1252.54	72	10	1230.36	78
11	1159.01	83	12	1078.01	78
13	1038.48	89	14	1008.59	84
15	992.196	86	16	959.412	81
17	937.235	83	18	887.095	86
19	856.239	76	20	812.849	75
21	781.029	73	22	757.888	77
23	746.317	75	24	669.178	78
25	616.145	79	26	577.576	78
27	527.436	75	28	488.866	68
29	470.546	74	30	438.726	81
31	423.298	80	32	405.942	74

Fig. S4. IR spectrum of complex **4**

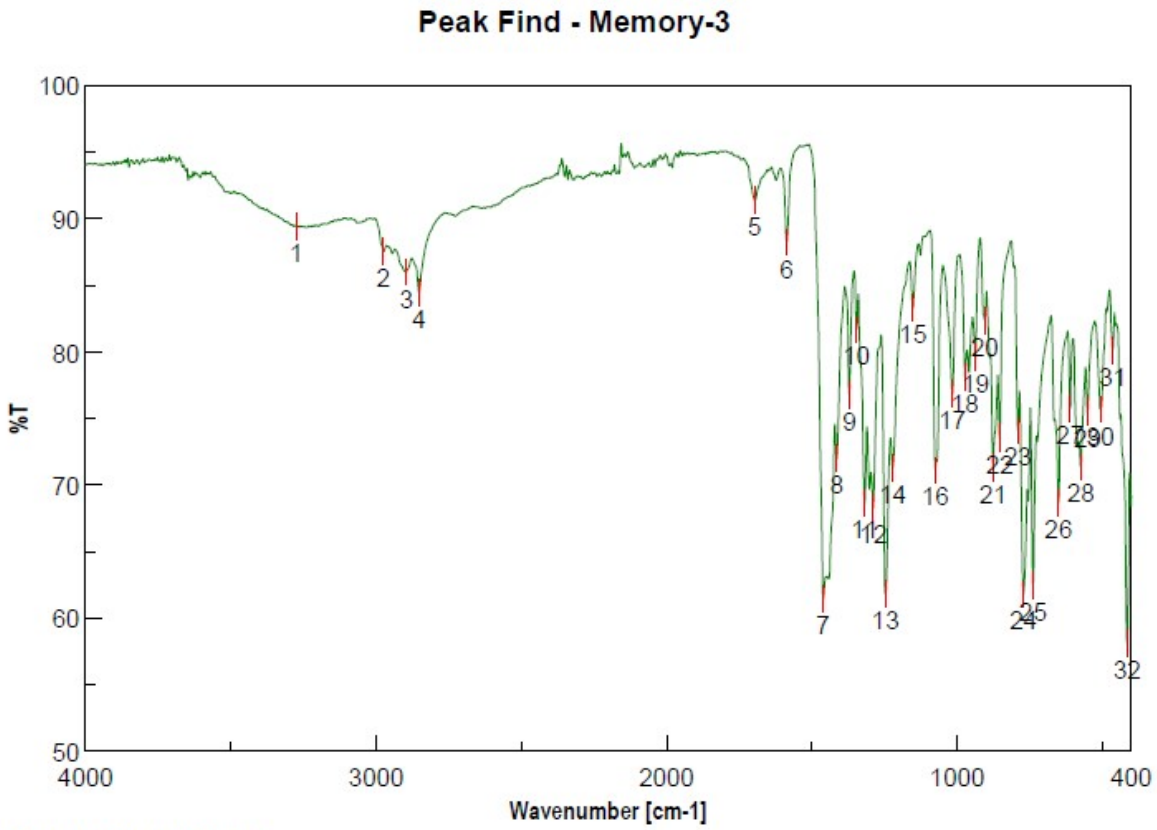

[Result of Peak Picking]

No.	Position	Intensity	No.	Position	Intensity
1	3274.54	89	2	2975.62	88
3	2896.56	86	4	2852.2	84
5	1697.05	91	6	1586.16	88
7	1460.81	61	8	1414.53	72
9	1371.14	77	10	1346.07	82
11	1318.11	69	12	1289.18	68
13	1246.75	62	14	1221.68	71
15	1152.26	83	16	1075.12	71
17	1016.3	77	18	972.912	78
19	937.235	80	20	904.451	82
21	876.488	71	22	853.347	74
23	790.671	74	24	771.387	62
25	738.603	62	26	650.858	69
27	611.324	76	28	574.683	71
29	551.542	75	30	506.223	76
31	463.796	80	32	414.62	58

Fig. S5. IR spectrum of complex **5**

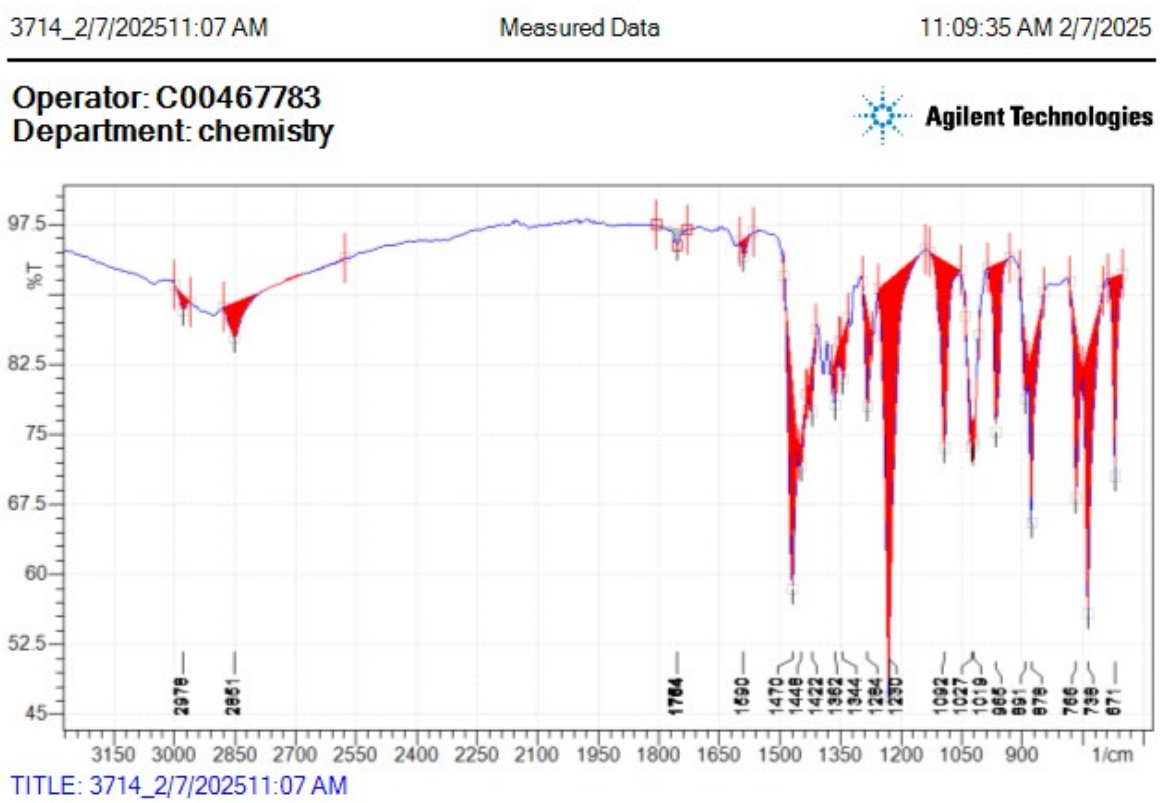

Fig. S6. IR spectrum of $\mathbf{H_4L^{Me,Cl}}$

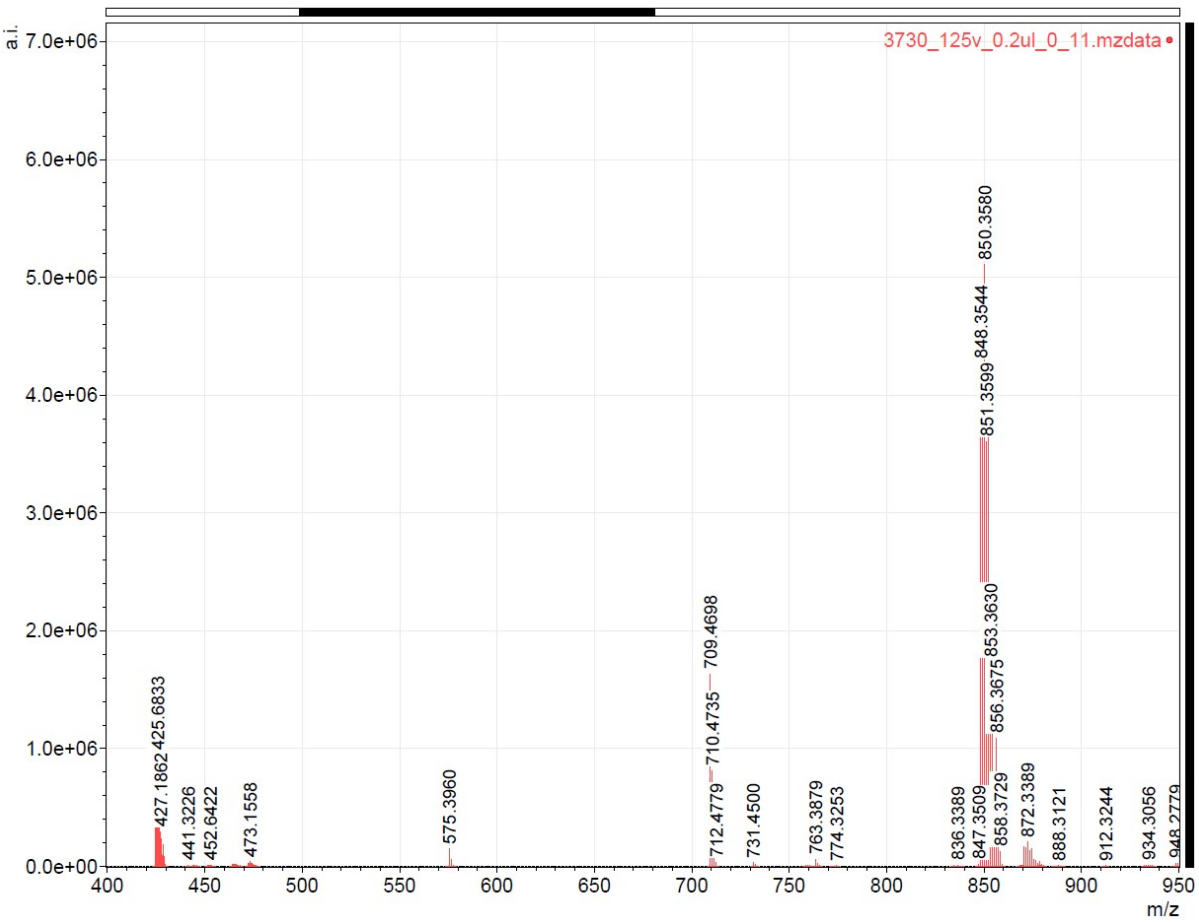

Fig. S7. ESI-MS of complex **1** in CH_3CN

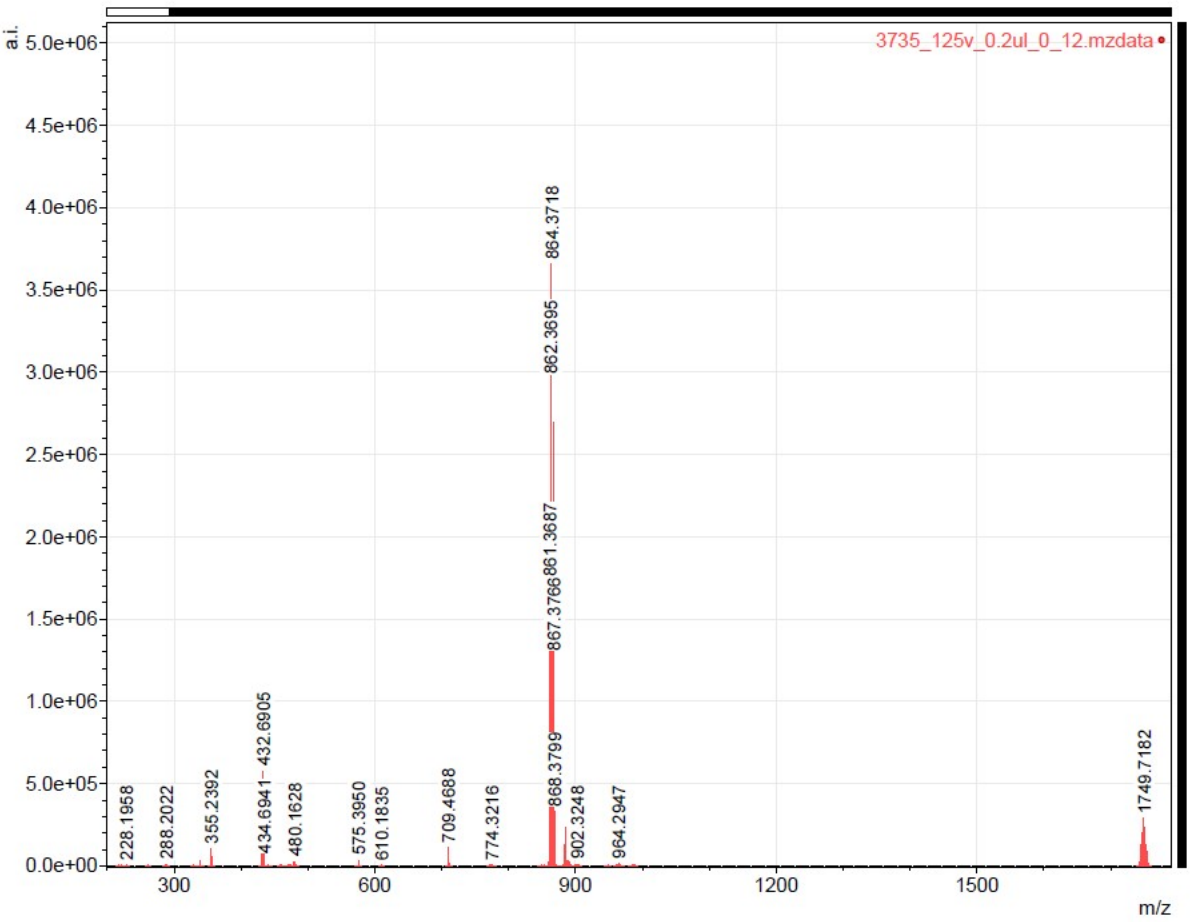

Fig. S8. ESI-MS of complex **2** in CH_3CN

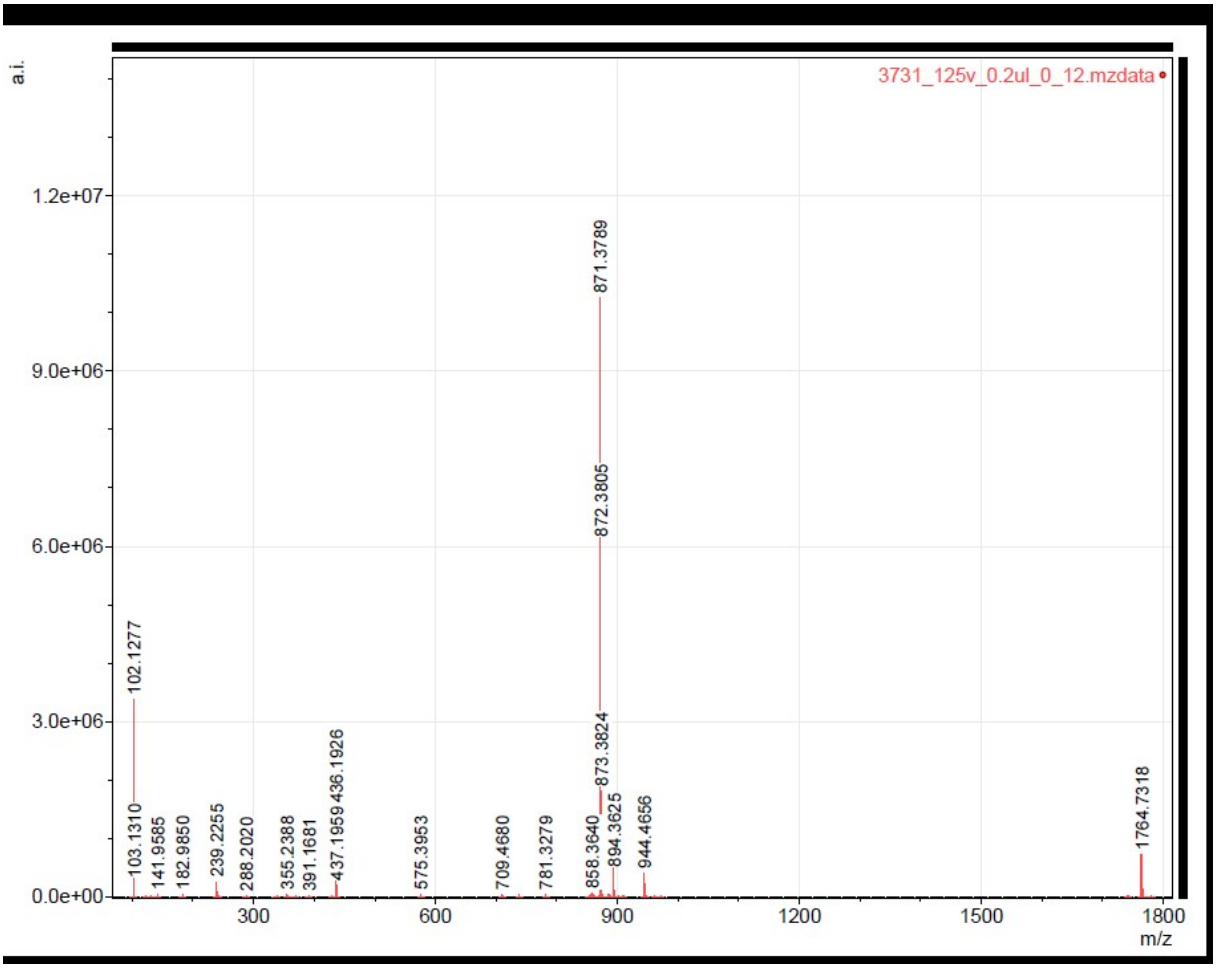

Fig. S9. ESI-MS of complex **4** in CH_3CN

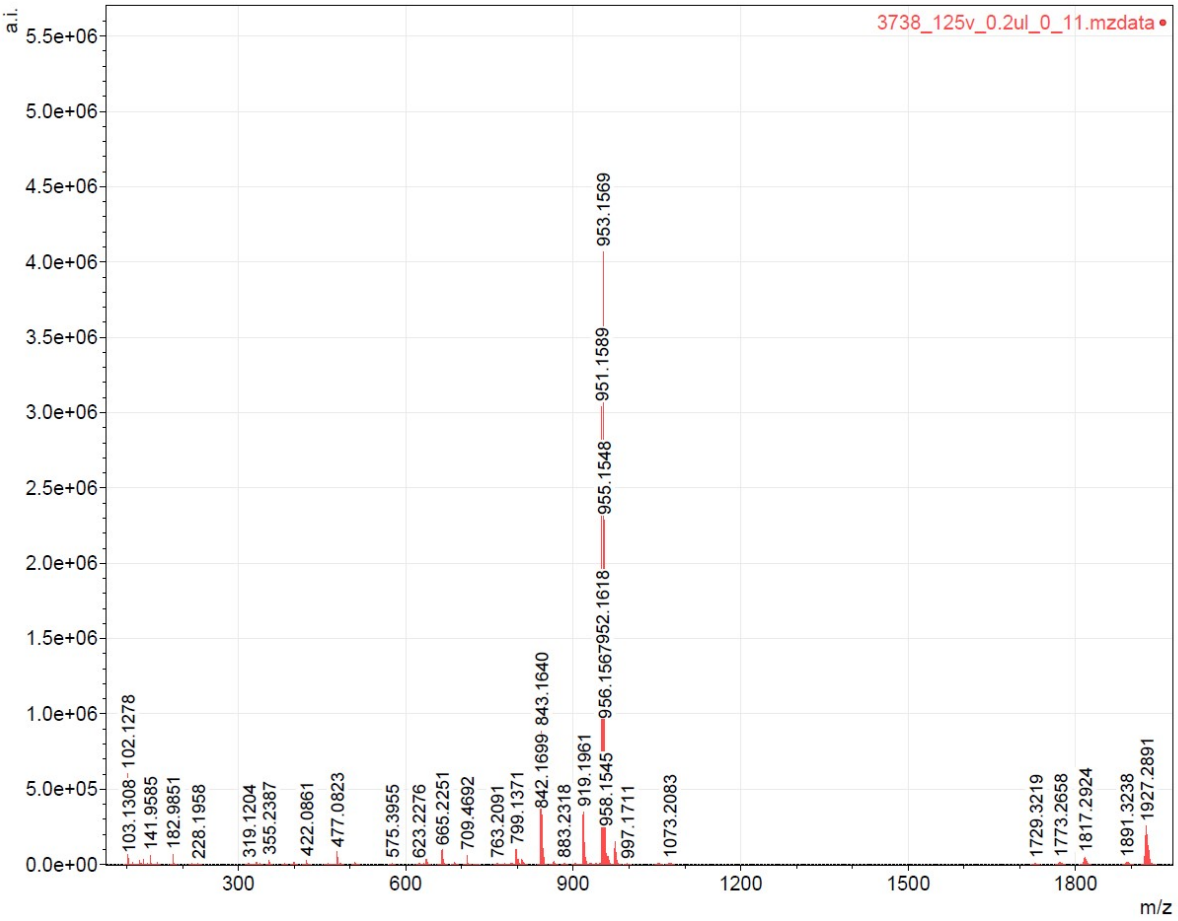

Fig. S10. ESI-MS of complex **5** in CH_3CN

Spectrum/Peak Report Date 9/9/2025 Time 08:53:43 Page 1 of 1

Method file : <method not saved>
Information : Default Method
Data File : C:\Chem32\1\DATA\3730AN.SD Created : 9/9/25 8:52:11

Overlaid Spectra:

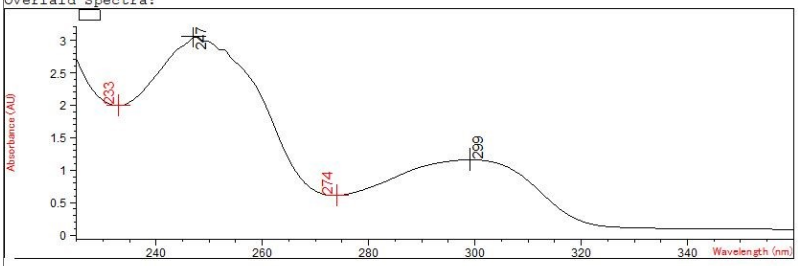

#	Name	Peaks(nm)	Abs(AU)	Valleys(nm)	Abs(AU)
1		247.0	3.05310	274.0	0.60734
1		299.0	1.16150	233.0	1.99160
1		***	***	***	***

Instrument S/N : CN22802974

Report generated by : ChemStationSystem Signature: .....

*** End Spectrum/Peak Report ***

Spectrum/Peak Report Date 9/9/2025 Time 09:00:06 Page 1 of 1

Method file : <method not saved>
Information : Default Method
Data File : C:\Chem32\1\DATA\3730AN(DIL).SD Created : 9/9/25 8:59:06

Overlaid Spectra:

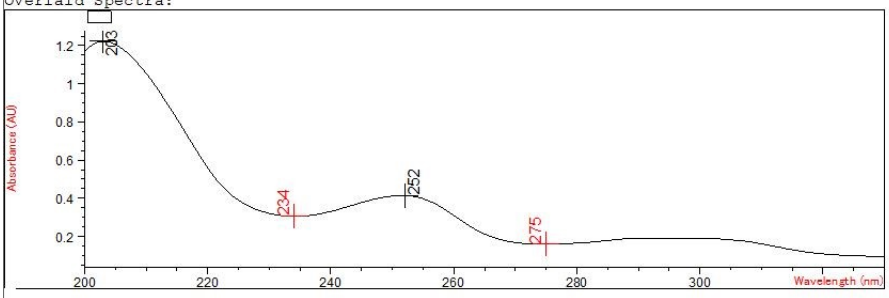

#	Name	Peaks(nm)	Abs(AU)	Valleys(nm)	Abs(AU)
1		203.0	1.22310	275.0	0.15817
1		252.0	0.41475	234.0	0.30510
1		***	***	***	***

Instrument S/N : CN22802974

Report generated by : ChemStationSystem Signature: .....

*** End Spectrum/Peak Report ***

Fig. S11. UV spectrum of complex **1** in CH_3CN (top:1.35 x 10^{-4} M; bottom: 1.35 x 10^{-5} M).

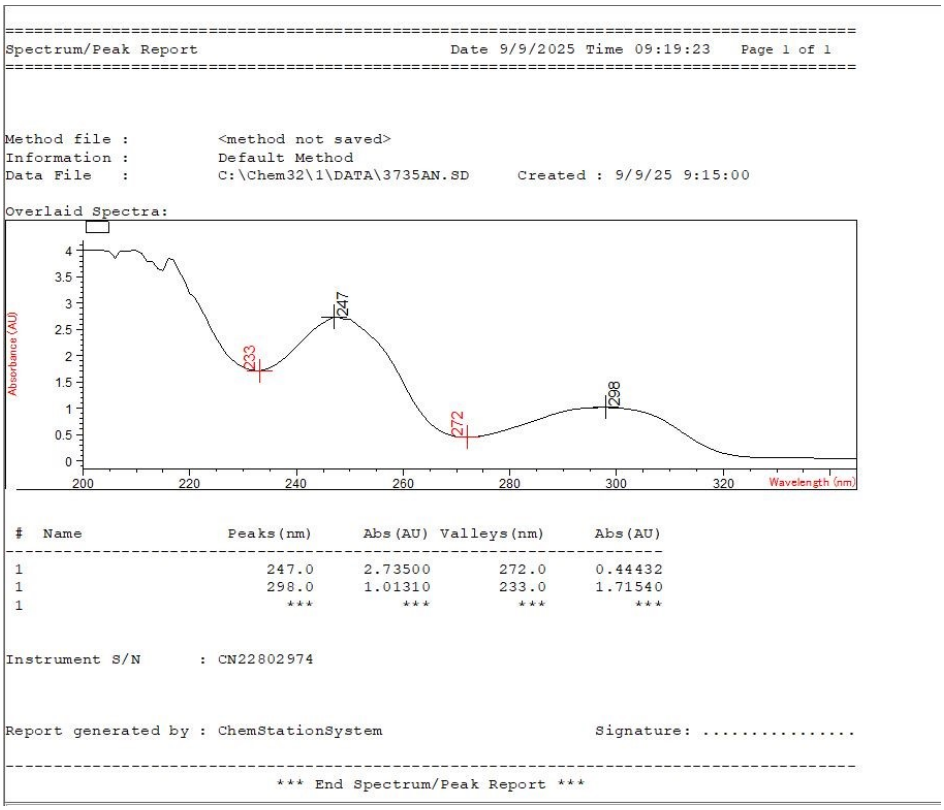

Spectrum/Peak Report — Date 9/9/2025 Time 09:19:23 Page 1 of 1

Method file : <method not saved>
Information : Default Method
Data File : C:\Chem32\1\DATA\3735AN.SD Created : 9/9/25 9:15:00

Overlaid Spectra:

#	Name	Peaks(nm)	Abs(AU)	Valleys(nm)	Abs(AU)
1		247.0	2.73500	272.0	0.44432
1		298.0	1.01310	233.0	1.71540
1		***	***	***	***

Instrument S/N : CN22802974

Report generated by : ChemStationSystem Signature: .....

*** End Spectrum/Peak Report ***

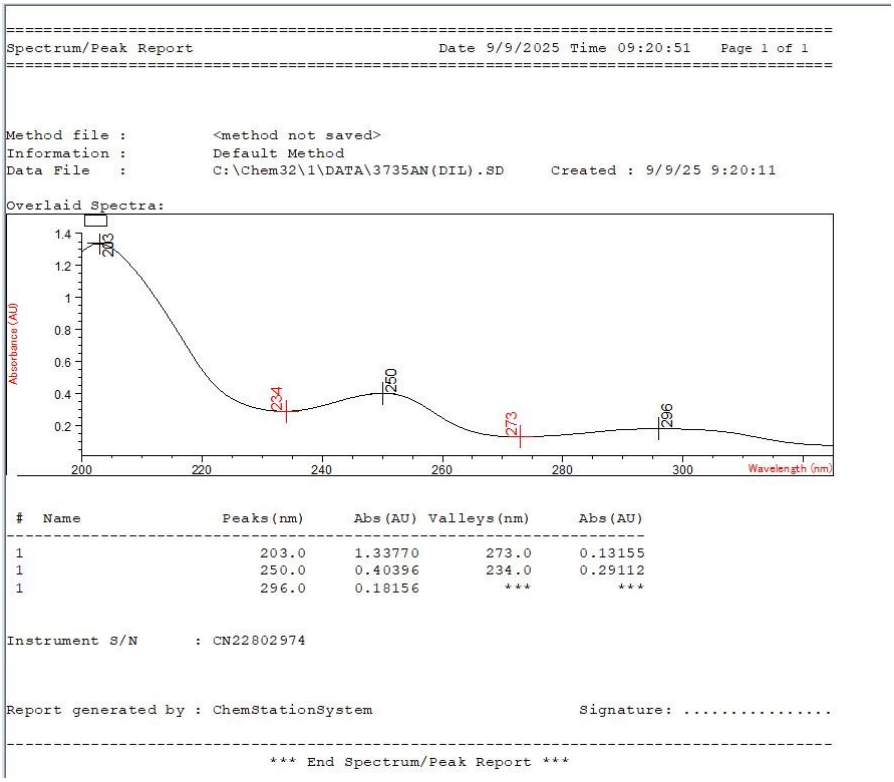

Spectrum/Peak Report — Date 9/9/2025 Time 09:20:51 Page 1 of 1

Method file : <method not saved>
Information : Default Method
Data File : C:\Chem32\1\DATA\3735AN(DIL).SD Created : 9/9/25 9:20:11

Overlaid Spectra:

#	Name	Peaks(nm)	Abs(AU)	Valleys(nm)	Abs(AU)
1		203.0	1.33770	273.0	0.13155
1		250.0	0.40396	234.0	0.29112
1		296.0	0.18156	***	***

Instrument S/N : CN22802974

Report generated by : ChemStationSystem Signature: .....

*** End Spectrum/Peak Report ***

Fig. S12. UV spectrum of complex **2** in CH_3CN (top:1.35 x 10^{-4} M; bottom: 1.35 x 10^{-5} M)

Spectrum/Peak Report Date 9/9/2025 Time 09:04:45 Page 1 of 1

Method file : <method not saved>
Information : Default Method
Data File : C:\Chem32\1\DATA\3738AN.SD Created : 9/9/25 9:03:33

Overlaid Spectra:

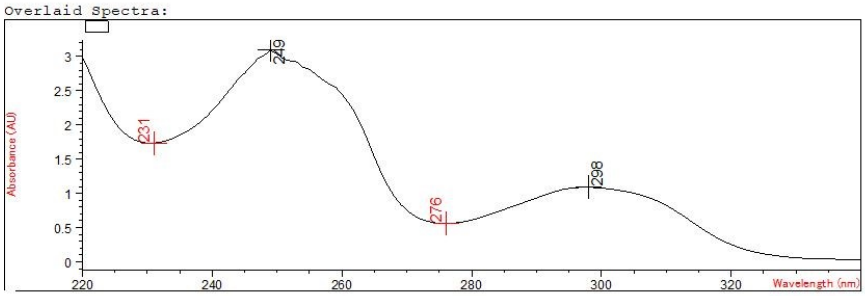

#	Name	Peaks(nm)	Abs(AU)	Valleys(nm)	Abs(AU)
1		249.0	3.09180	276.0	0.55907
1		298.0	1.08920	231.0	1.73450
1		***	***	***	***

Instrument S/N : CN22802974

Report generated by : ChemStationSystem Signature: .....

*** End Spectrum/Peak Report ***

Spectrum/Peak Report Date 9/9/2025 Time 09:10:38 Page 1 of 1

Method file : <method not saved>
Information : Default Method
Data File : C:\Chem32\1\DATA\3738AN(DIL).SD Created : 9/9/25 9:09:52

Overlaid Spectra:

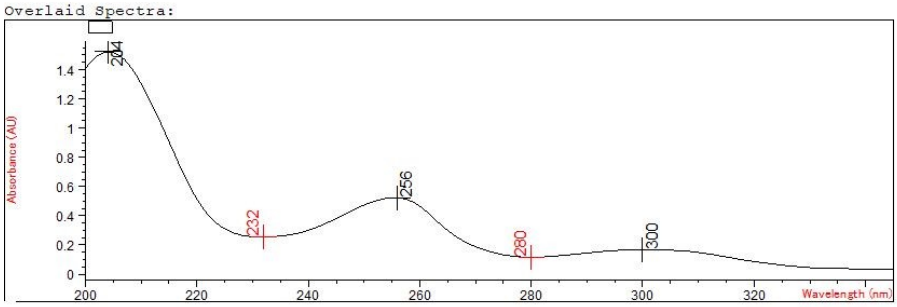

#	Name	Peaks(nm)	Abs(AU)	Valleys(nm)	Abs(AU)
1		204.0	1.52250	280.0	0.11598
1		256.0	0.52314	232.0	0.25359
1		300.0	0.16645	***	***

Instrument S/N : CN22802974

Report generated by : ChemStationSystem Signature: .....

*** End Spectrum/Peak Report ***

Fig. S13. UV spectrum of complex **5** in CH_3CN (top:1.35 x 10^{-4} M; bottom: 1.35 x 10^{-5} M)

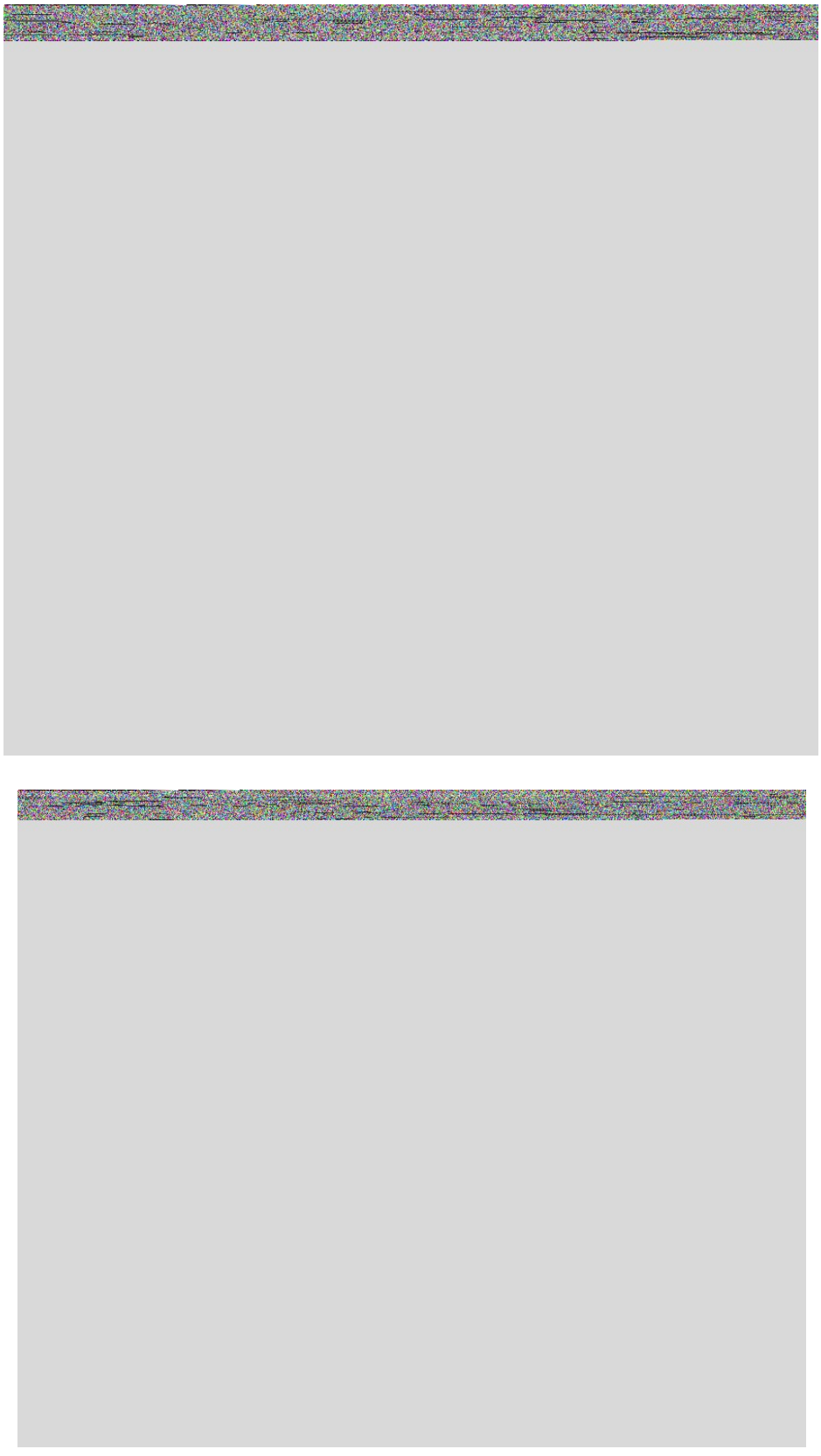

Fig. S14. UV spectrum of $H_4L^{Cl,Me}$ in CH_3CN (top:1.35 x 10^{-4} M; bottom: 1.35 x 10^{-5} M).

Table S1. Crystallographic data and details of measurements for compounds **1, 2, 4** and **5**
R1= $\Sigma/ |F_o|- |F_c|/|\Sigma|F_d$; wR2 = $[\Sigma_w(F_o^2-F_2^2)^2/\Sigma_w(F_o^2)^2]^{1/2}$

Compound	$[Nd(HL^{Me,Me})]\cdot MeOH$ (**1**)	$[Gd(HL^{Me,Me})]\cdot MeOH$ (**2**)	$[Ho(HL^{Me,Me})]\cdot MeOH$ (**4**)	$[Ho(HL^{Me,Cl})]\cdot 2MeOH$ (**5**)
CCDC No.	2489782	2489783	2489784	2489785
Formula	$C_{44}H_{57}N_4NdO_4\cdot CH_4O$	$C_{44}H_{57}GdN_4O_4\cdot CH_4O$	$C_{44}H_{57}HoN_4O_4\cdot CH_4O$	$C_{42}H_{53}Cl_4HoN_4O_6$
Fw (g mol^{-1})	882.21	895.22	902.90	1016.61
a (Å)	14.8343(6)	14.8229(4)	14.9515(7)	13.1871(6)
b (Å)	12.4668(5)	12.4491(4)	12.4578(6)	18.6904(8)
c (Å)	22.4721(9)	22.4326(8)	22.3763(11)	17.0530(6)
α (°)	90	90	90	90
β (°)	90	90	90	102.217(2)
γ (°)	90	90	90	90
V (Å^3)	4155.9(3)	4139.5(2)	4167.9(3)	4107.9(3)
Z	4	4	4	4
Crystal size (mm)	0.09 × 0.07 × 0.06	0.15 × 0.1 × 0.08	0.17 × 0.13 × 0.09	0.17 × 0.14 × 0.08
Crystal habit	Block, light blue	Block, colourless	Block, green	Block, green
Crystal system	Orthorhombic	Orthorhombic	Orthorhombic	Monoclinic
Space group	$Pca2_1$	$Pca2_1$	$Pca2_1$	$P2_1/n$
d_{calc} (Mg m^{-3})	1.410	1.436	1.439	1.598
μ (mm^{-1})	1.30	1.65	1.95	2.24
Radiation type	Mo K_α	Mo K_α	Mo K_α	Mo K_α
Wavelength (Å)	0.71073	0.71073	0.71073	0.71073
T (K)	100(2)	100(2)	100(2)	100(2)
θ range (°)	2.3–33.1	2.4–28.3	2.3–27.9	2.4–27.9
F(000)	1836	1852	1864	2000
T_{min}, T_{max}	0.622, 0.747	0.477, 0.746	0.542, 0.746	0.616, 0.746
R_{int}	0.098	0.103	0.101	0.080
No. of measured, independent and observed [$I > 2\sigma(I)$] reflections	203178, 15842, 14048	112309, 112309, 8798	235200, 10760, 9522	81536, 9945, 8019
independent reflections	15842	112309	10760	9945
No. of parameters, restraints	514, 1	507, 1	507, 1	533, 0
Δρmax, Δρmin (e Å^{-3})	1.31, -1.14	1.46, -3.67	0.85, -1.05	0.74, -1.14
GooF	1.06	1.05	1.04	1.04
Absolute structure parameter	0.030(9)	0.011(7)	0.028(5)	—
R1, wR2 (all	R1 = 0.0347	R1 = 0.0528	R1 = 0.0365	R1 = 0.0506

data)	wR2 = 0.0614	wR2 = 0.0734	wR2 = 0.0614	wR2 = 0.0590
R1, wR2 ($>2\sigma$)	R1 = 0.0265 wR2 = 0.0575	R1 = 0.0409 wR2 = 0.0698	R1 = 0.0274 wR2 = 0.0572	R1 = 0.0327 wR2 = 0.0550

Table S2. Bond lengths and angles around metal centers in compounds **1-5**.

	1, M=Nd	**2**, M=Gd	**3**, M=Tb	**4**, M=Ho	**5**, M=Ho
M(III)-N1 (Å)	2.730(5)	2.666(5)	2.660(4)	2.660(4)	2.597(3)
M(III)-N2 (Å)	2.682(5)	2.663(5)	2.641(4)	2.646(3)	2.631(3)
M(III)-N3 (Å)	2.703(6)	2.686(5)	2.651(4)	2.617(4)	2.578(3)
M(III)-N4 (Å)	2.746(5)	2.688(5)	2.668(4)	2.637(4)	2.608(3)
M(III)-O1 (Å)	2.199(5)	2.198(4)	2.146(3)	2.138(3)	2.201(2)
M(III)-O2 (Å)	2.286(4)	2.240(4)	2.226(3)	2.203(3)	2.201(3)
M(III)-O3 (Å)	2.231(4)	2.162(4)	2.170(3)	2.170(3)	2.129(2)
N1-M(III)-N2 (°)	67.33(15)	69.42(16)	69.1(1)	68.12(10)	70.71(9)
N2-M(III)-N3 (°)	69.15(18)	67.80(15)	69.6(1)	70.07(11)	68.92(9)
N3-M(III)-N4 (°)	66.51(16)	67.28(15)	68.6(1)	69.22(11)	69.41(9)
N4-M(III)-N1 (°)	66.03(17)	67.85(15)	67.3(1)	68.29(11)	70.67(9)
O1-M(III)-O2 (°)	96.85(16)	93.98(15)	93.6(1)	94.04(12)	89.88(9)
O2-M(III)-O3 (°)	96.33(16)	95.17(15)	94.8(1)	91.52(11)	91.88(10)
O3-M(III)-O1 (°)	93.01(16)	91.53(16)	86.9(1)	90.33(11)	89.18(9)

Table S3. Coordination geometries of metal centers in compounds **1-5**.

Compound	{N1>N4} plane* RMSD (Å)	{N1>N4} - M(III) (Å)[a]	O1>O3 - M(III) (Å)[a]	{N1>N4} – M(III) – {O1>O3} (Å)[b]	{N1>N4} - M(III) - {O1>O3} (°)[b]	O1>O3 to plane twist angle (°)	{O1>O3} to {N1>N4} plane fold angle (°)
1	0.013	1.6953(11)	1.1624(11)	2.8536(15)	173.76(7)	116(2)	4.29(6)
2	0.012	1.63533(3)	1.18820(2)	2.81630(6)	174.53(5)	124.88(7)	4.47667(4)
3	0.010	1.603(2)	1.2201(18)	2.820(3)	174.62(11)	107(2)	4.49(11)
4	0.010	1.5834(17)	1.2092(17)	2.790(2)	175.41(11)	111(3)	4.27(10)
5	0.014	1.5252(16)	1.2497(16)	2.772(2)	175.06(9)	128(2)	5.37(9)

* MPLN – Olex2[7], { N1>N4} refers to plane spanned by coordinated N atoms, { O1>O4} to phenolate O-atoms

[a] plane centroid to metal

[b] plane centroid to metal to plane centroid

Table S4. SHAPE analyses for compounds **1, 2, 4** and **5**.

Compounds		Shape calculations						
		HP-7 (D_{7h})	HPY-7 (C_{6v})	PBPY-7 (D_{5h})	COC-7 (C_{3v})	CTPR-7 (C_{2v})	JPBPY-7 (D_{5h})	JETPY-7 (C_{3v})
(1)·CH_3OH	Nd1	35.537	19.284	6.224	1.438	1.850	10.594	21.314
(2)·CH_3OH	Gd1	35.665	19.162	6.165	1.269	1.630	10.364	21.070
(4)·CH_3OH	Ho1	35.382	19.211	6.243	1.243	1.308	10.281	20.781
(5)·2CH_3OH	Ho1	35.709	19.090	6.038	0.904	1.647	10.059	20.534

*HP-7 corresponds to an Heptagon, HPY-7 to an Hexagonal pyramid, PBPY-7 to a Pentagonal bipyramid, COC-7 to a Capped octahedron, CTPR-7 to a Capped trigonal prism, JPBPY-7 to a Johnson pentagonal bipyramid J13 and JETPY-7 to a Johnson elongated triangular pyramid J7.

Table S5. Possible hydrogen bonds for compound **1.**

D—H···*A*	*D*—H	H···*A*	*D*···*A*	*D*—H···*A*
O4—H4O···O5	0.72(4)	1.99(5)	2.659(3)	154(5)
O5—H5*A*···O2^{i}	0.81(5)	2.01(5)	2.807(3)	171(5)
C10—H10*B*···O3^{ii}	0.97	2.56	3.453 (3)	153
C38—H38*B*···O5^{iii}	0.97	2.59	3.487 (4)	154
C43—H43*B*···O4	0.97	2.36	3.047 (3)	128
C45—H45*A*···O4	0.96	2.59	3.059 (5)	110

Symmetry codes: (i) *x*, *y*+1, *z*; (ii) *x*-1/2, -*y*, *z*; (iii) *x*-1/2, -*y*+1, *z*.

* D = Donor, A = Acceptor.

a)

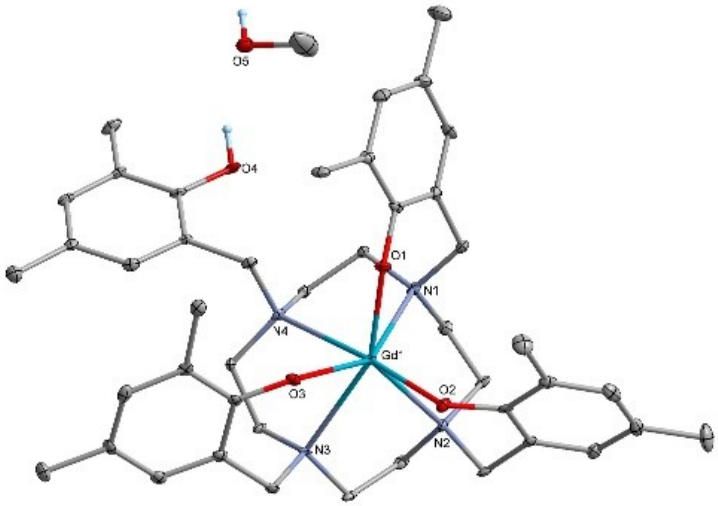

b)

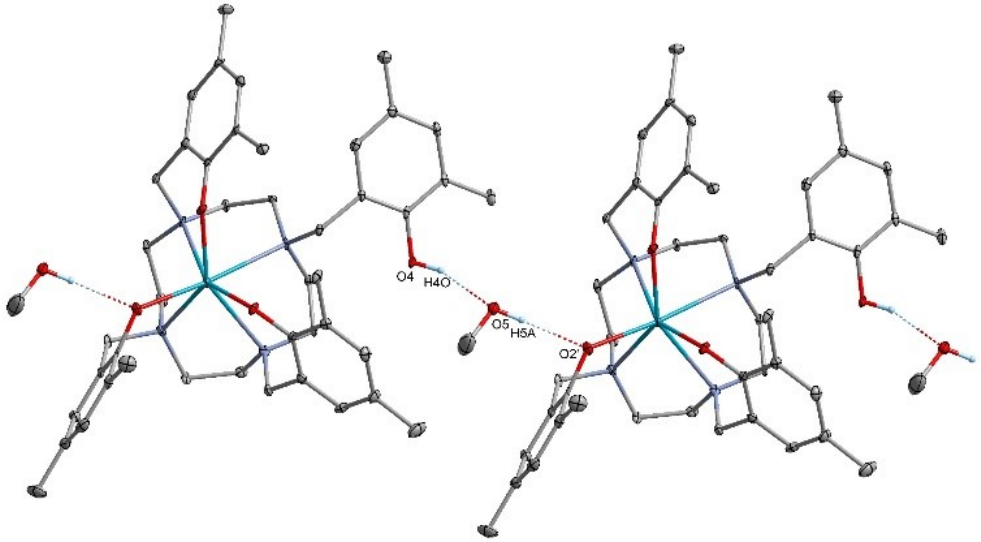

Fig. S15. a) Perspective view and b) Crystal packing of **2**.

a)

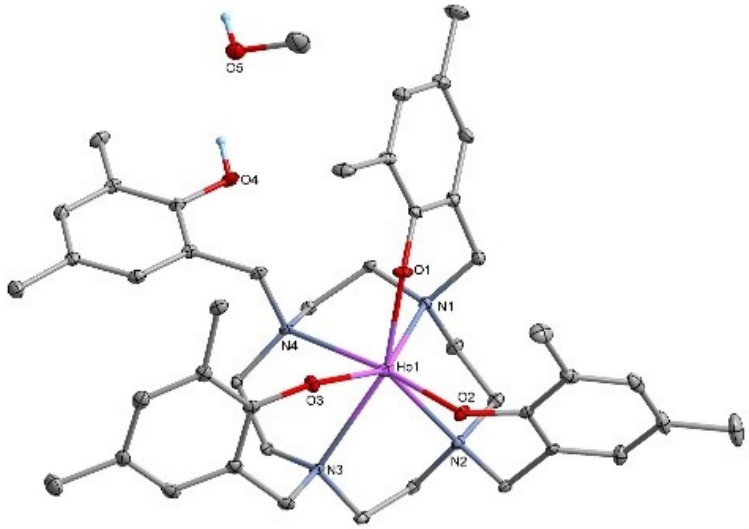

b)

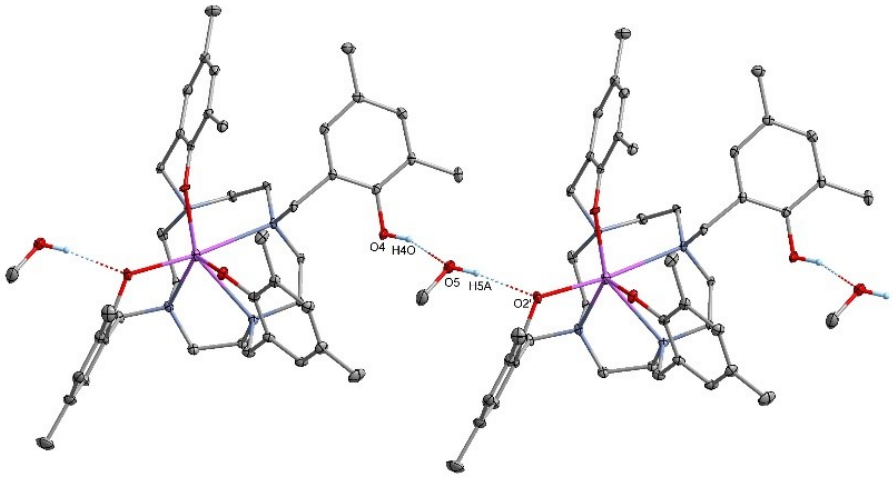

Fig. S16. a) Perspective view and b) Crystal packing of **4**.

a)

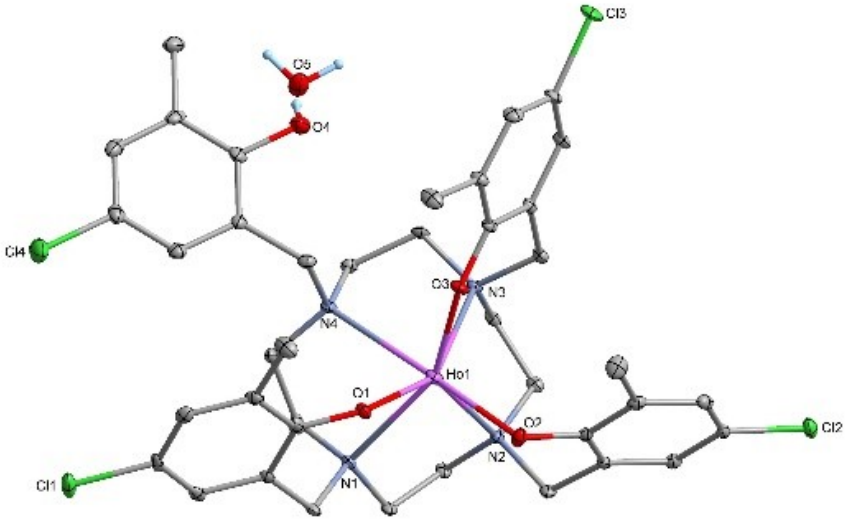

b).

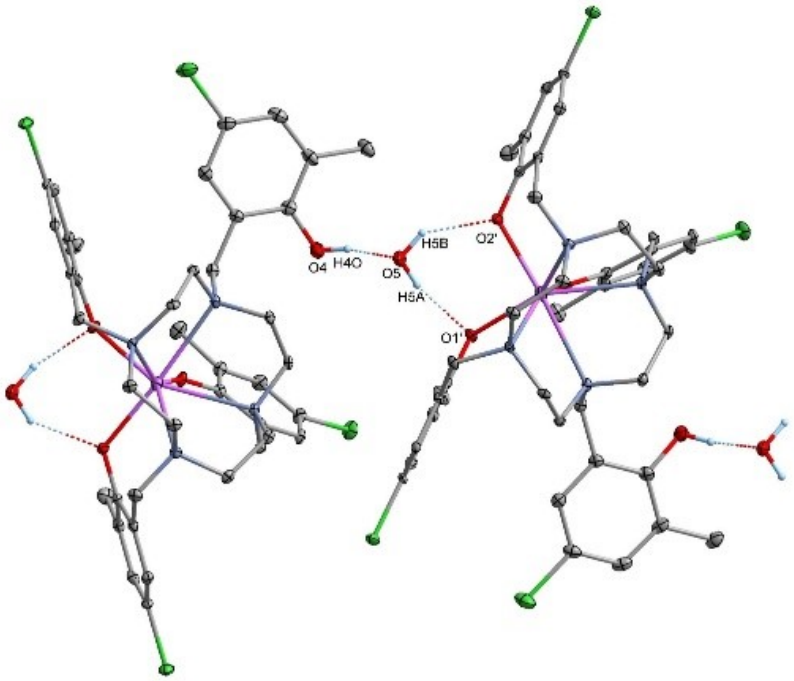

Fig. S17. a) Perspective view and b) Crystal packing of **5**

Table S6. Possible hydrogen bonds for compound **2.**

D—H···*A*	*D*—H	H···*A*	*D*···*A*	*D*—H···*A*
O4—H4O···O5	0.84	1.85	2.661(6)	160.8
O5—H5*A*···O2^{i}	0.84	1.98	2.821(6)	174.0
C12—H12A···O3^{ii}	0.99	2.58	3.501(7)	154.6
C11—H11B···O5^{iii}	0.99	2.55	3.455(8)	152.6
C43—H43B···O4	0.99	2.33	3.048(7)	128.3

Symmetry codes: (i) *x*, -1+*y*, *z*; (ii) 1/2+*x*, 2-*y*, *z*; (iii) 1/2+*x*, 1-*y*, *z*.

Table S7. Possible hydrogen bonds for compound **4.**

D—H···*A*	*D*—H	H···*A*	*D*···*A*	*D*—H···*A*
O4—H4O···O5	0.84	1.87	2.659(5)	156
O5—H5*A*···O2^{ii}	0.84	1.99	2.820(5)	171
C43—H43*A*···O4	0.99	2.36	3.085(5)	129
C11—H11*A*···O5^{i}	0.99	2.57	3.441(6)	147
C34—H34*B*···O3	0.99	2.59	3.332(5)	131

Symmetry codes: (i) *x*, *y*-1, *z*; (ii) *x*+1/2, -*y*+1, *z*.

Table S8. Possible hydrogen bonds for compound **5.**

D—H···*A*	*D*—H	H···*A*	*D*···*A*	*D*—H···*A*
O4—H4O···O5	0.84	1.71	2.506(7)	157
O5—H5*A*···O1^{i}	0.87	1.91	2.768(6)	150
O5—H5*B*···O2^{ii}	0.87	2.05	2.733(6)	135
C20—H20*B*···Cl1^{i}	0.99	2.86	3.793(4)	157
C30—H30*A*···Cl2^{iii}	0.99	2.99	3.842(4)	145
C30—H30*B*···O4	0.99	2.49	3.147(5)	123
C40—H40*B*···Cl1^{iv}	0.99	2.96	3.681(4)	131
C7—H7···Cl4^{iv}	0.95	2.94	3.841(4)	158
C31—H31*A*···O1	0.99	2.66	3.374(5)	130
C31—H31*B*···O3	0.99	2.62	3.122(5)	112
C35—H35···O7	0.95	2.52	3.389(7)	152

Symmetry codes: (i) 1/2+*x*, 1/2-*y*, 1/2+*z*; (ii) *x*+1/2, -*y*+1/2, *z*+1/2; (iii) -*x*+3/2, *y*-1/2, -*z*+1/2; (iv) -*x*+1, -*y*, -*z*.

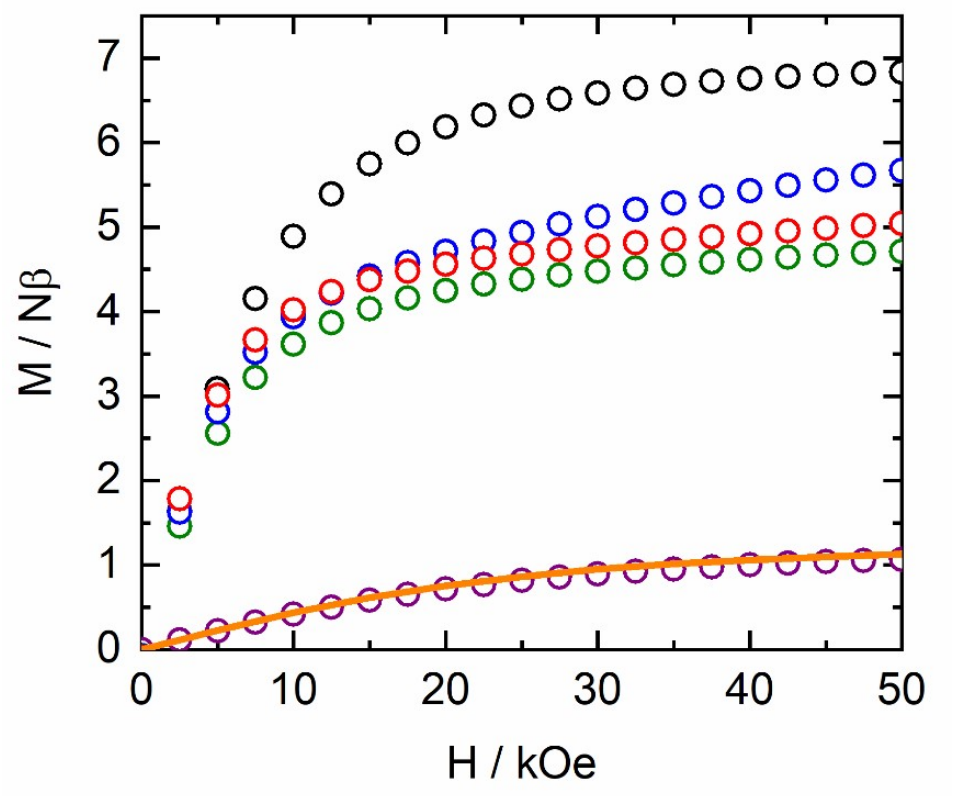

Fig. S18. Field dependence of the magnetization at 2 K in the 0-50 kOe field range for **1** (purple), **2** (black), **3** (green), **4** (red) and **5** (blue). Full orange line corresponds to calculated data.

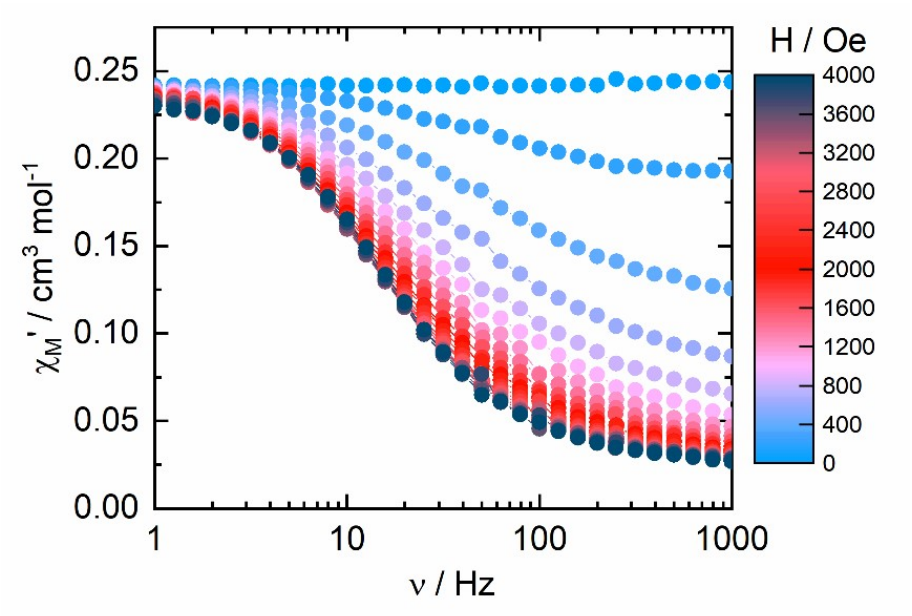

Fig. S19. Field dependence of the in-phase component of the magnetic susceptibility at 2 K in the 0-4000 Oe field range for **1**.

Extended Debye model (Eq. S1).

$$\chi_M' = \chi_S + (\chi_T - \chi_S)\frac{1+(\omega\tau)^{1-\alpha}\sin\left(\alpha\frac{\pi}{2}\right)}{1+2(\omega\tau)^{1-\alpha}\sin\left(\alpha\frac{\pi}{2}\right)+(\omega\tau)^{2-2\alpha}}$$

$$\chi_M'' = (\chi_T - \chi_S)\frac{(\omega\tau)^{1-\alpha}\cos\left(\alpha\frac{\pi}{2}\right)}{1+2(\omega\tau)^{1-\alpha}\sin\left(\alpha\frac{\pi}{2}\right)+(\omega\tau)^{2-2\alpha}}$$

With χ_T the isothermal susceptibility, χ_S the adiabatic susceptibility, τ the relaxation time and α an empiric parameter which describe the distribution of the relaxation time. For SMM with only one relaxation time, α is close to zero. The extended Debye model was applied to fit simultaneously the experimental variations of χ_M' and χ_M'' with the frequency ν of the oscillating field ($\omega = 2\pi\nu$). Typically, only the temperatures for which a maximum on the χ'' vs. ν curves, have been considered. The best fitted parameters τ, α, χ_T, χ_S are listed in Tables S6 and S7 with the coefficient of determination R^2.

Table S7. Best fitted parameters (χ_T, χ_S, τ and α) with the extended Debye model for compound **1** at 2 K in the field range 0-4000 Oe.

H / Oe	χ_S / cm^3 mol^{-1}	χ_T / cm^3 mol^{-1}	τ / s	α	R^2
200	0.18994	0.24233	0.00302	0.25836	0.99994
400	0.11702	0.24619	0.0035	0.32863	0.99991
600	0.07726	0.24999	0.00451	0.33621	0.99968
800	0.05789	0.25158	0.00555	0.32487	0.99935
1000	0.04708	0.2522	0.00629	0.31275	0.99919
1200	0.04101	0.25051	0.00695	0.29346	0.99899
1400	0.03719	0.25048	0.00754	0.28326	0.99925
1600	0.03464	0.25007	0.00817	0.2707	0.99929
1800	0.03284	0.24914	0.00873	0.25988	0.99936
2000	0.03161	0.24813	0.00926	0.25139	0.99925
2200	0.03082	0.24808	0.00958	0.24732	0.99918
2400	0.02937	0.24594	0.00986	0.22955	0.99928
2600	0.02935	0.24585	0.01023	0.22911	0.99916
2800	0.02832	0.24395	0.01024	0.22144	0.99936
3000	0.02761	0.24242	0.01024	0.21213	0.99944
3200	0.02855	0.24659	0.01012	0.21801	0.99925
3400	0.02803	0.24475	0.01001	0.20695	0.99953
3600	0.02704	0.2425	0.00969	0.19424	0.99962
3800	0.02757	0.24106	0.00942	0.19016	0.99914
4000	0.02681	0.23857	0.00901	0.17753	0.9996

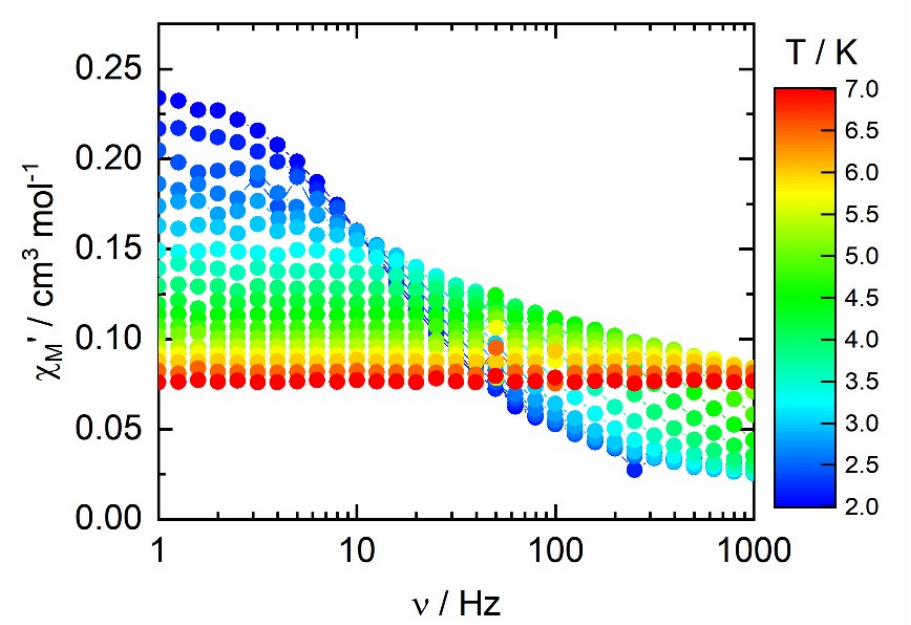

Fig. S20. Temperature dependence of the in-phase component of the magnetic susceptibility under an applied field of 3200 Oe in the 2-7 K temperature range for **1**.

Table S8. Best fitted parameters (χ_T, χ_S, τ and α) with the extended Debye model for compound **1** at 3200 Oe in the temperature range 2-5.1 K.

T / K	χ_S / cm^3 mol^{-1}	χ_T / cm^3 mol^{-1}	τ / s	α	R^2
2	0.02793	0.24652	0.01084	0.21976	0.99942
2.2	0.02698	0.22594	0.00891	0.19813	0.99923
2.4	0.02593	0.20262	0.00669	0.17597	0.99761
2.6	0.02569	0.18965	0.00528	0.15619	0.99827
2.8	0.02376	0.1782	0.00405	0.15263	0.99905
3	0.02367	0.16505	0.00297	0.11943	0.99941
3.3	0.0235	0.15027	0.00185	0.08438	0.99937
3.6	0.023	0.13938	0.00118	0.07371	0.99973
3.9	0.02147	0.12906	7.20313E-4	0.06354	0.99919
4.2	0.02243	0.1208	4.59435E-4	0.03693	0.99971
4.5	0.01997	0.11403	2.89834E-4	0.0275	0.99878
4.8	0.02303	0.10694	1.91928E-4	0.01937	0.99933
5.1	0.02394	0.10181	1.29749E-4	0.01017	0.99886

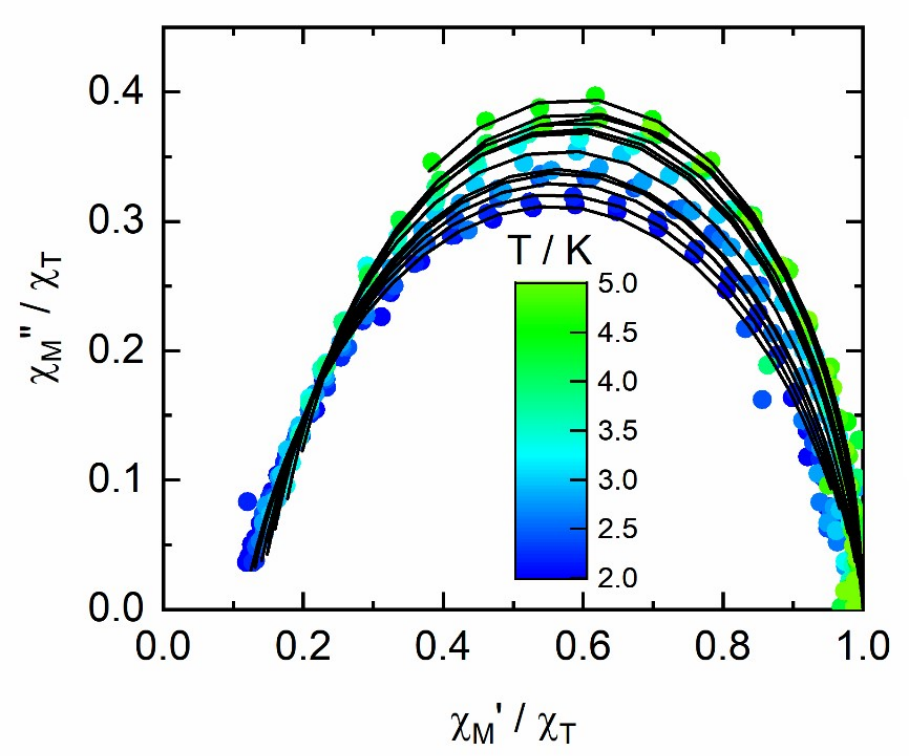

Fig. S21. Normalized Argand plot for **1** in the 0-5.1 K temperature range.

Table S9. SINGLE_ANISO computed energy barrier and angles between the g_{zz} axes of KDs.

Energy (cm^{-1})	g_{xx}	g_{yy}	g_{zz}	θ
0.0	1.09	1.61	3.50	-
91.0	2.74	2.63	0.09	52.8
174.4	0.31	1.56	3.30	42.2
268.6	0.41	0.57	5.68	105.9
503.5	1.84	2.42	3.62	75.9

Table S10. SINGLE_ANISO computed Cystal-Field parameters B_k^q for the complex **1**.

k	q	B_k^q
2	-2	-1.0899
2	-1	0.0465
2	0	-0.5075
2	1	-1.6063
2	2	0.4716
4	-4	-0.0564
4	-3	0.2230
4	-2	0.0307
4	-1	0.0613

4	0	0.0103
4	1	-0.0468
4	2	0.0456
4	3	0.1004
4	4	-0.0462

Table S11. Decomposition of the RASSI wave functions corresponding to the lowest atomic multiplet *J=9/2* in wave functions with definite projection of the total moment on the quantization axis for the states of the complex **1**.

m_J	ab initio state 1		ab initio state 2	
	Real	Imaginary	Real	Imaginary
-9/2	-0.118526	0.451748	0.105851	-0.403439
-7/2	0.160579	-0.093461	0.167131	0.160105
-5/2	-0.143755	-0.411600	0.061136	0.283856
-3/2	0.100695	-0.087969	-0.070898	-0.059466
-1/2	0.199503	-0.164648	-0.382028	-0.078312
1/2	0.021203	-0.389395	0.209888	-0.151187
3/2	0.039526	0.083668	-0.110644	0.075074
5/2	0.259048	0.131172	0.361642	0.243505
7/2	-0.112449	-0.202291	-0.131153	0.131603
9/2	-0.417094	0.000000	-0.467038	0.000000
	ab initio state 3		ab initio state 4	
-9/2	0.065050	0.123192	-0.143071	-0.270948
-7/2	0.068861	-0.037134	-0.400359	-0.322437
-5/2	-0.046484	0.191334	0.074343	-0.366326
-3/2	-0.262170	0.392669	-0.124652	0.225656
-1/2	0.131079	-0.022509	-0.263676	-0.247491
1/2	-0.341974	-0.117603	-0.041302	-0.126422
3/2	-0.141340	0.215596	0.224815	-0.415187
5/2	-0.289225	0.236792	-0.147489	0.130447
7/2	0.472071	0.203474	-0.000683	0.078233
9/2	-0.306402	0.000000	-0.139312	0.000000

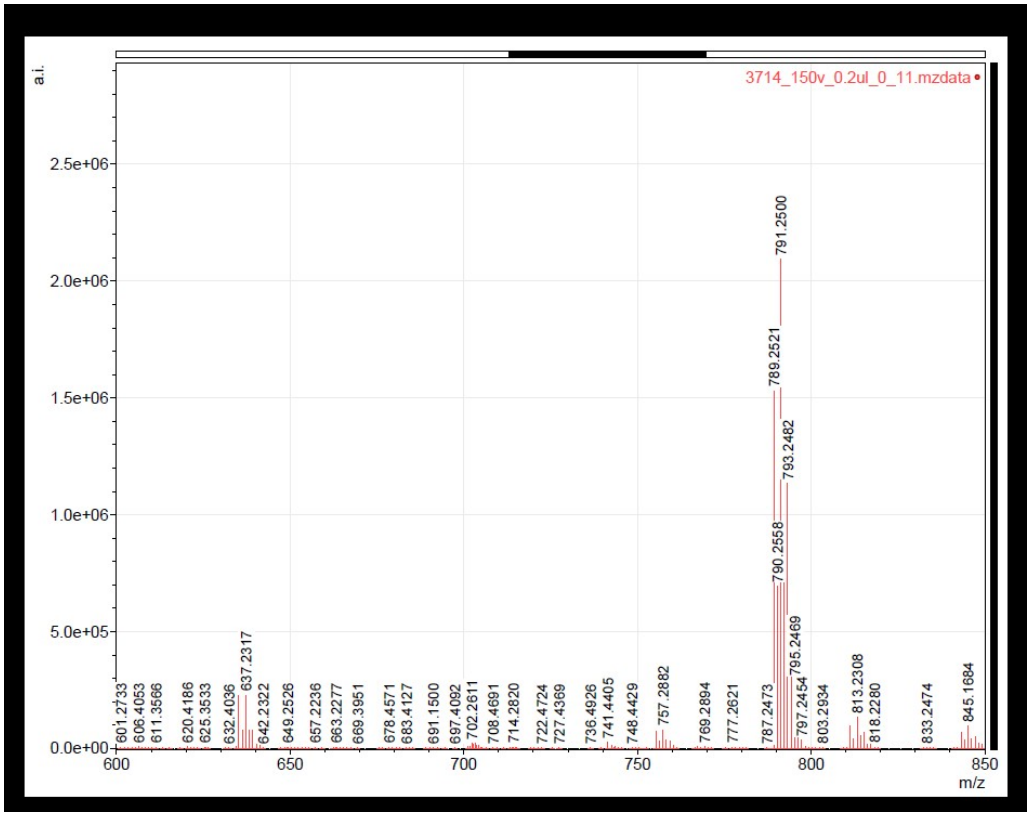

Fig. S22. ESI-MS of $\mathbf{H_4L^{Me,Cl}}$ in MeOH

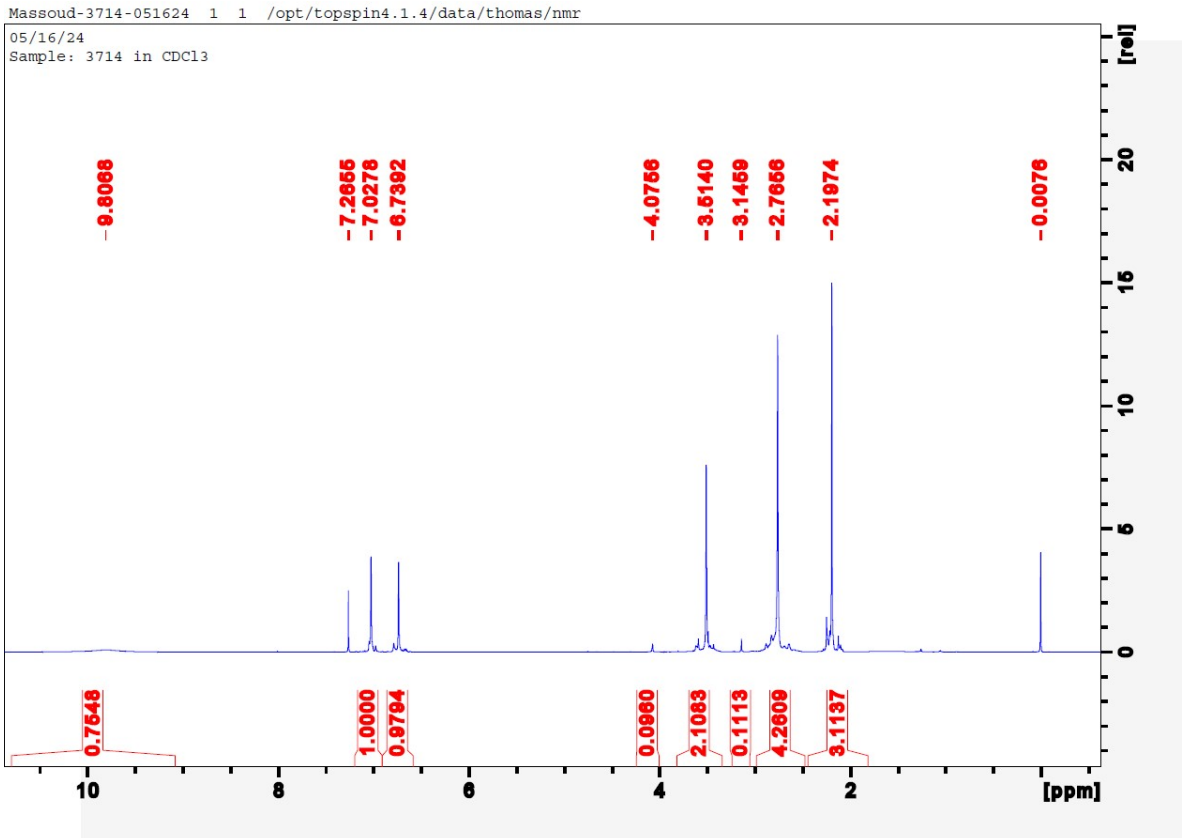

Fig. S23. ^{1}H NMR of $\mathbf{H_4L^{Me,Cl}}$ in $CDCl_3$